Advanced Composite Materials
Publication details, including instructions for authors and subscription information:
http://www.tandfonline.com/loi/tacm20

High-cycle fatigue characteristics of quasi-isotropic CFRP laminates

Atsushi Hosoi [a], Yoshihiko Arao [b], Hirokazu Karasawa [c] & Hiroyuki Kawada [d]

[a] Graduate School of Science and Engineering, Waseda University, 3-4-1, Okubo, Shinjuku-ku, Tokyo 169-8555, Japan

[b] Graduate School of Science and Engineering, Waseda University, 3-4-1, Okubo, Shinjuku-ku, Tokyo 169-8555, Japan

[c] Toshiba Corporation Industrial and Power Systems and Services Company,1-1-1, Shibaura, Minato-ku, Tokyo 105-8001, Japan

[d] Department of Mechanical Engineering, Waseda University, 3-4-1, Okubo, Shinjuku-ku, Tokyo 169-8555, Japan

Version of record first published: 02 Apr 2012.

To cite this article: Atsushi Hosoi , Yoshihiko Arao , Hirokazu Karasawa & Hiroyuki Kawada (2007): High-cycle fatigue characteristics of quasi-isotropic CFRP laminates, Advanced Composite Materials, 16:2, 151-166

To link to this article: http://dx.doi.org/10.1163/156855107780918964

Adv. Composite Mater., Vol. 16, No. 2, pp. 151–166 (2007)

Also available online - www.brill.nl/acm

High-cycle fatigue characteristics of quasi-isotropic CFRP laminates

ATSUSHI HOSOI [1,*], YOSHIHIKO ARAO [1], HIROKAZU KARASAWA [2] and HIROYUKI KAWADA [3]

[1] *Graduate School of Science and Engineering, Waseda University, 3-4-1, Okubo, Shinjuku-ku, Tokyo 169-8555, Japan*
[2] *Toshiba Corporation Industrial and Power Systems and Services Company,1-1-1, Shibaura, Minato-ku, Tokyo 105-8001, Japan*
[3] *Department of Mechanical Engineering, Waseda University, 3-4-1, Okubo, Shinjuku-ku, Tokyo 169-8555, Japan*

Received 26 April 2006; accepted 26 July 2006

Abstract—High-cycle fatigue characteristics of quasi-isotropic carbon fiber reinforced plastic (CFRP) laminates $[-45/0/45/90]_s$ up to 10^8 cycles were investigated. To assess the fatigue behavior in the high-cycle region, fatigue tests were conducted at a frequency of 100 Hz, since it is difficult to investigate the fatigue characteristics in high-cycle at 5 Hz. Then, the damage behavior of the specimen was observed with a microscope, soft X-ray photography and a 3D ultrasonic inspection system. In this study, to evaluate quantitative characteristics of both transverse crack propagation and delamination growth in the high-cycle region, the energy release rate associated with damage growth in the width direction was calculated. Transverse crack propagation and delamination growth in the width direction were evaluated based on a modified Paris law approach. The results revealed that transverse crack propagation delayed under the test conditions of less than $\sigma_{max}/\sigma_b = 0.3$ of the applied stress level.

Keywords: Polymer–matrix composites; transverse cracking; delamination; high-cycle fatigue; energy release rate.

1. INTRODUCTION

CFRPs are expected to replace metal materials and aid the expansion of applications in various fields in the future since they have excellent mechanical properties, such as lightness, high strength and good moldability. However, structures under serviced loads suffer from fatigue failures, and it is noted that high-cycle fatigue fractures

Edited by the JSCM.

*To whom correspondence should be addressed. E-mail: atsushi_h@moegi.waseda.jp

are the main cause of the destruction of the structures. In particular, components used in cars and high-speed trains are subjected to a cyclic loading of over 10^8 cycles. Therefore, the long-term reliability of CFRP laminates must be established. Moreover, in many applications, CFRP is used in the form of multidirectional laminates. Hence, it is important to investigate the high-cycle fatigue characteristics of quasi-isotropic CFRP laminates.

Fatigue characteristics of CFRP and glass fiber reinforced plastics (GFRP) laminates have been investigated in previous studies [1–7]. Especially, it is important to investigate the transverse crack growth behavior to establish the long-term reliability, because transverse cracks initiate in a laminate first and cause delamination. Many studies to date have been conducted to predict the behavior of transverse crack growth in composite laminates under tensile loadings [8–13]. Moreover, from fatigue tests on various types of CFRP cross-ply laminates, Liu and Nairn [14] showed that the transverse crack density growth rate could be expressed as a function of the energy release rate range derived by the variational principle. Takeda *et al.* [15] conducted fatigue tests to determine the effects of toughened interlaminar layers with quasi-isotropic CFRP laminates by evaluating the transverse crack density growth rate and the delamination ratio growth rate as a function of the energy release rate range. Yokozeki *et al.* [16] studied transverse cracks propagating in the width direction of specimens with several CFRP cross-ply laminates and quasi-isotropic laminates. They showed that the derived energy release rate was independent of the crack length, and the transverse crack growth in the width direction could be evaluated as a function of the energy release rate range.

However, all these studies have investigated fatigue characteristics of CFRP laminates up to 10^6 cycles from the viewpoint of the transverse crack and delamination analysis. Therefore, in the present study, the propagation behaviors of the transverse crack and delamination were investigated in high-cycle fatigue up to 10^8 cycles. To observe this damage, a microscope, soft X-ray photography and a 3D ultrasonic inspection system were used. The energy release rate associated with transverse crack and delamination growth was respectively calculated, and the quantitative damage characteristics were investigated in this study.

2. EXPERIMENTAL

2.1. Materials

The material system used in this study was T700S/2500. The stacking sequence of laminates was $[-45/0/45/90]_S$. The specimen geometry is shown in Fig. 1. All specimens were 210 mm long, 30 mm wide, and 1.0 mm thick with 55 mm GFRP end-tabs leaving a 100 mm gauge section. Young's modulus and tensile strength of the laminates were 45.3 GPa and 826 MPa, respectively. The mechanical properties of the specimen are shown in Table 1.

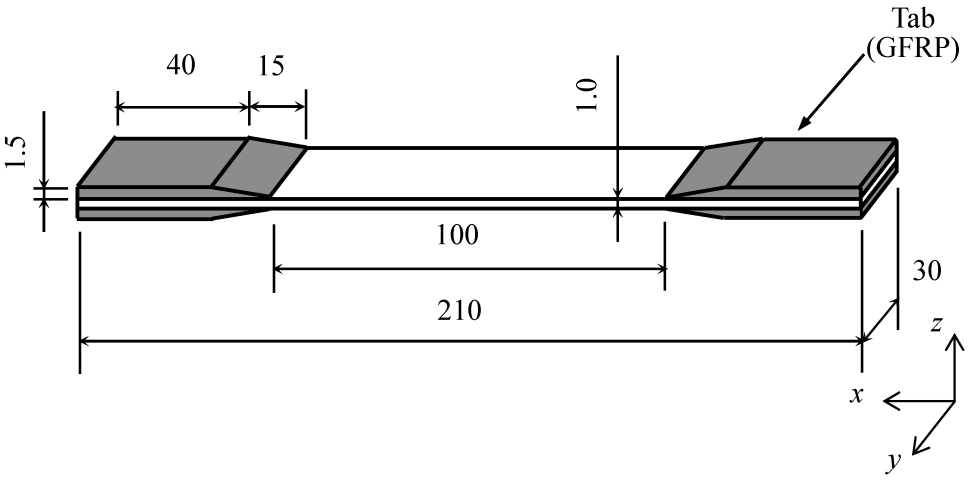

Figure 1. Specimen geometry used in fatigue tests.

Table 1.
Mechanical properties of T700S/2500 unidirectional composite

Longitudinal Young's modulus (GPa)	131.2
Transverse Young's modulus (GPa)	9.25
In-plane shear modulus (GPa)	3.5
In-plane Poisson's ratio	0.37
Out-of-plane Poisson's ratio	0.49*
Longitudinal thermal expansion coefficient ($\times 10^{-6}$/K)	0.3
Transverse thermal expansion coefficient ($\times 10^{-6}$/K)	36.5
Manufacturing temperature (K)	403

* Assumed value.

2.2. Fatigue tests

Tensile fatigue tests were conducted at room temperature with a sine waveform under load control conditions using a hydraulic-driven testing machine. All tests were run at a stress ratio of $R = 0.1$ and the selected maximum stress levels were 20–60% of the static tensile strength, σ_b. In case of the fatigue tests at a frequency of 5 Hz, the applied stress level was set within $\sigma_{max}/\sigma_b = 0.2$–$0.6$. At a frequency of 100 Hz, the applied stress level was set within $\sigma_{max}/\sigma_b = 0.2$–$0.3$ to control the specimen temperature rising under fatigue tests.

2.3. Damage observation

The damage behavior was observed in detail with three kinds of equipment. First, the transverse crack and the delamination that initiated at specimen edges were observed by a microscope. Then, the transverse crack and the delamination which propagated inside the specimen were observed by soft X-ray photography. Finally,

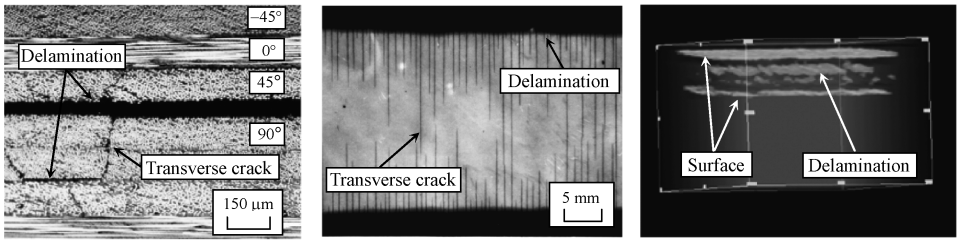

(a) Damage at specimen edge (b) Internal damage of specimen (c) 3D damage behavior

Figure 2. Damage behavior observed with (a) microscope, (b) soft X-ray photography and (c) 3D ultrasonic inspection system.

the internal state of the specimen was observed by a 3D ultrasonic inspection system. The representative photos are shown in Fig. 2.

3. EFFECTS OF SPECIMEN TEMPERATURE UNDER FATIGUE TESTS

3.1. Measurement of specimen temperature change under fatigue tests

The prepreg of CFRP has mechanical and thermal anisotropy, so it is known that the anisotropy influences the fracture mechanism of the laminates. This is because residual thermal stress is caused by the variation in test temperatures from the curing temperature in the specimen. Moreover, it is predicted that the temperature of the specimen rises due to visco-elastic characteristics during the fatigue test at a frequency of 100 Hz. Hence, the temperature change in each test condition was measured with an infrared temperature sensor.

Figure 3 shows the results of the temperature change of the specimen. From these results, a remarkable temperature rise was observed under the test conditions of a frequency of 100 Hz and an applied stress level of $\sigma_{\max}/\sigma_{\mathrm{b}} = 0.4$. It was then observed that the temperature of the specimen remained constant after 150 s.

3.2. Prediction of temperature distribution inside specimen

Figure 3 shows the results of monitoring the temperature variation of the specimen surface. Hence, it is necessary to investigate the temperature distribution through the thickness of the specimen. In this study, the distribution was predicted with a one-dimensional heat conduction equation under fatigue tests. In the analysis, the model that the specimen heated uniformly on the inside and was cooled down on the surfaces was considered. Then, it was assumed that the heat moved in one direction, i.e., z direction in Fig. 4(a). The assumption indicates that the specimen is adequately long and wide compared to its thickness, and heat radiation is ignored in the fixed portion of specimen tabs and the edges of the specimen. In Fig. 4(b), B, T and T_f indicate specimen thickness, specimen temperature and environmental temperature, respectively. The stacking sequence of laminates used in this study

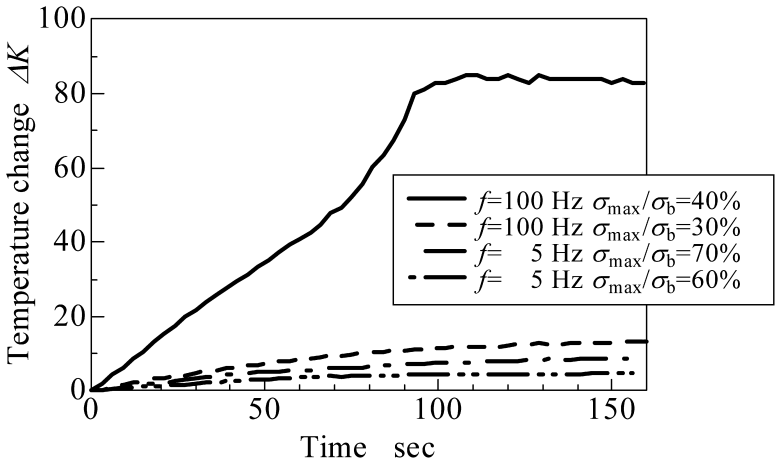

Figure 3. Temperature change of specimen surface subjected to cyclic loading under frequencies of 5 Hz and 100 Hz.

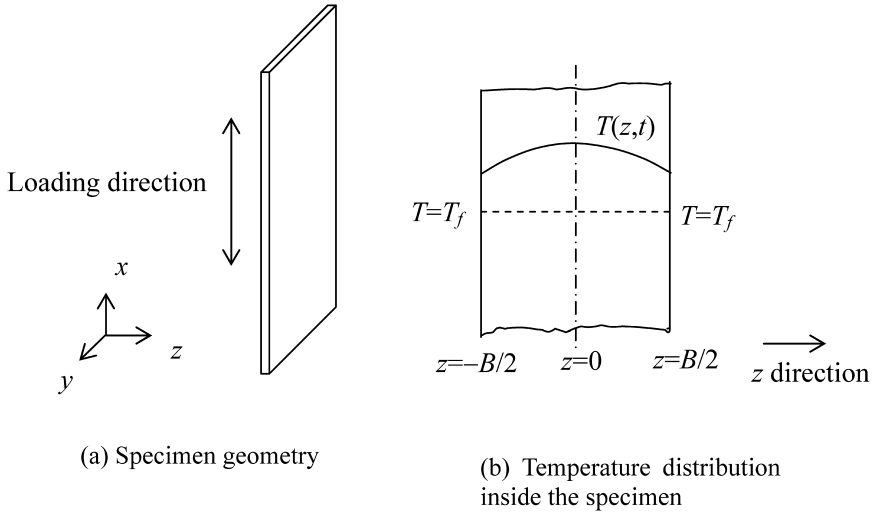

Figure 4. Model of temperature distribution in 1 dimension.

is $[-45/0/45/90]_S$ and accordingly it is thought that the heat generation inside the specimen is not uniform. However, the specimen was considered to be isotropic in order to predict the temperature distribution of the specimen easily.

The one-dimensional steady state heat conduction equation associated with internal heat generation is expressed as

$$\left(\frac{\partial^2 T}{\partial z^2}\right) + \frac{\dot{q}_v}{\lambda} = 0, \tag{1}$$

where $\dot{q}_v$ and λ indicate the calorific potential per unit volume and the thermal conductivity, respectively. Equation (1) can be solved with the following boundary

conditions. Considering the symmetry at $z = 0$, and the calorific potential at $z = B/2$, the boundary conditions are expressed as

$$\frac{\mathrm{d}T}{\mathrm{d}z} = 0 \quad (\text{at } z = 0), \quad -\lambda\frac{\mathrm{d}T}{\mathrm{d}z} = \alpha(T - T_f) \quad (\text{at } z = B/2), \tag{2}$$

where α shows the heat transfer coefficient. When the equation (1) is solved under these conditions, the temperature of the specimen is calculated as

$$T = \frac{\dot{q}_\mathrm{v}}{2\lambda}\left(\frac{B^2}{4} - z^2\right) + \frac{\dot{q}_\mathrm{v}B}{2\alpha} + T_f. \tag{3}$$

When the calorific potential is equal to the energy loss due to the visco-elastic characteristics, energy loss per unit volume and per cycle ΔE is expressed as

$$\Delta E = \int_0^{2\pi/\omega} \sigma(t) \cdot \mathrm{d}\varepsilon(t) = \pi E'' \varepsilon_0^2. \tag{4}$$

When a fatigue test is conducted at the frequency f, the calorific potential per unit volume is calculated as

$$\dot{q}_v = f\Delta E = \pi f E'' \varepsilon_0^2. \tag{5}$$

From equation (5), it was clear that the internal heat generation under the fatigue test increased in proportion to the frequency and to the square of the applied strain. Therefore, it is thought that the remarkable temperature rise was observed at a frequency of 100 Hz with the applied stress level of $\sigma_{\max}/\sigma_\mathrm{b} = 0.4$ as shown in Fig. 3. The loss modulus E'' varies according to the frequency or the temperature, so the loss modulus E'' was measured to calculate the calorific potential at a frequency of 5 Hz or 100 Hz. Figure 5 shows the results of measuring the visco-elastic characteristics under tension.

As shown in Fig. 5, compared to frequency, it is found that the results at a frequency of 100 Hz shift to higher temperature. However, the values of loss modulus by about 340 K are almost the same regardless of the frequency. Therefore, the effect of visco-elastic characteristics due to frequency is small in test temperatures from room temperature to 340 K. The temperature distribution inside the specimen during the fatigue test was predicted from the result shown in Fig. 5 and equations (3) and (5). The values used in the analysis are shown in Table 2.

Figure 6 shows the results of predicting the temperature distribution inside the specimen under the fatigue test condition with the applied stress level of $\sigma_{\max}/\sigma_\mathrm{b} = 0.3$ when the temperature of the specimen surface is constant. The results show that the temperature difference between the specimen surface and inside is greater when the frequency is greater. However, the temperature difference between the specimen surface and inside was negligible, at only 0.4 K. Considering the temperature rise of the specimen surface and the temperature distribution inside the specimen as shown in Figs 3 and 6, the applied stress level was set at less than

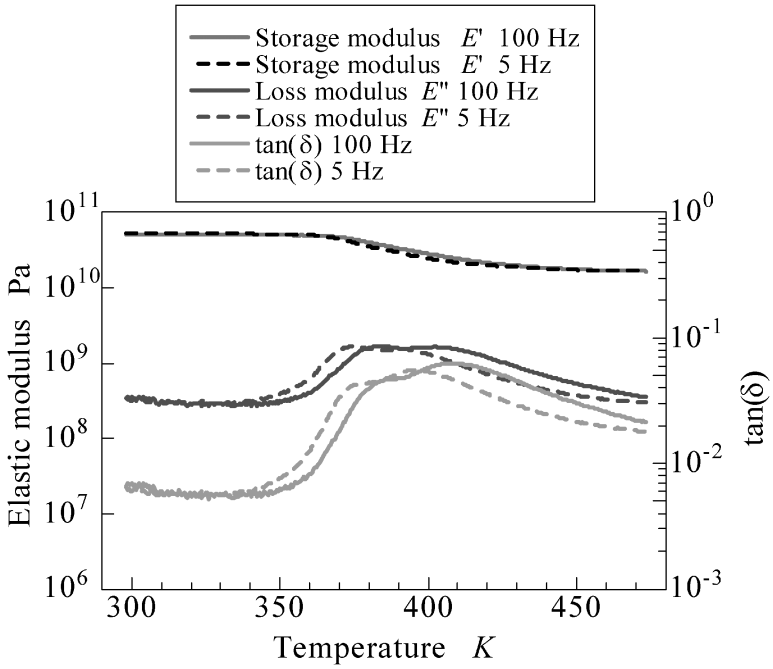

Figure 5. Storage modulus, loss modulus and tan(δ) as a function of temperature at frequencies of 100 Hz and 5 Hz.

Table 2.
Values used to calculate temperature distribution

Frequency (Hz)	5, 100
Loss modulus (N/m^2)	28.6×10^7
Thermal conductivity (W/mK)	0.637
Specimen thickness (m)	1.0×10^{-3}

$\sigma_{max}/\sigma_b = 0.3$ when the fatigue test was conducted at a frequency of 100 Hz in this study.

4. EXPERIMENTAL RESULTS AND DISCUSSION

4.1. Behavior of transverse crack propagation

The quasi-isotropic CFRP laminates show a highly complex fracture mode as follows [17]. In the primary stage of the fatigue test, transverse cracks were initiated in the 90 deg ply. Afterwards, delamination occurred in the interlaminar area of the 45/90 deg plies or the 90/90 deg plies. Almost simultaneous with the initiation of delamination, matrix cracks were initiated in the 45 deg ply from the tip of the transverse crack of the 90 deg ply. Then, the transverse crack of the 90 deg ply and the delamination propagated to the width direction of the specimen, after

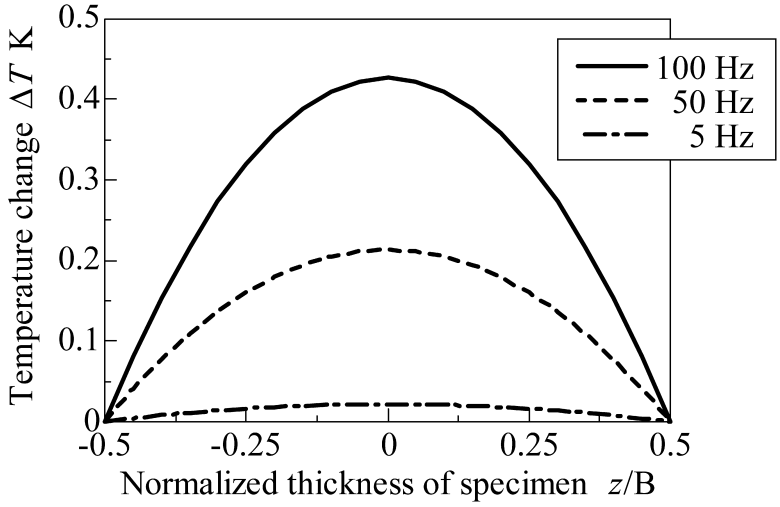

Figure 6. Prediction of temperature distribution inside specimen by difference in frequency.

the transverse cracks had saturated at the edge of the specimen. Moreover, matrix cracks of the −45 deg were observed at the edge. Finally, the specimen radically fractured by the fibers breaking in the 0 deg ply.

In this study, a key focus was the transverse crack propagation in the 90 deg ply. The behavior of transverse crack growth is shown Figs 7 and 8. Figure 7 shows the transverse crack density initiated at the specimen edge as a function of the normalized fatigue life predicted with the S–N curve. Figure 8 shows the normalized transverse crack length propagated in the width direction of the specimen as a function of normalized fatigue life. From the two graphs, it was found that the transverse crack propagated in the width direction of the specimen once it saturated at the specimen edge. The schematic illustration of the transverse crack growth behavior is shown in Fig. 9.

From the experimental results shown in Fig. 7, it was clear that the saturation value of the transverse crack density was different depending on the applied stress level. Under an applied stress level of 40% to 60%, the saturation value of the transverse crack was about 1.5 mm^{-1}. However, under an applied stress level of 30%, the saturation value was about 1.0 mm^{-1}. Moreover, the initiation of the transverse crack was delayed under the applied stress levels of 30% and 20%. From the experimental results shown in Fig. 8, it was found that the transverse cracks that were initiated at the specimen edges propagated to the width direction as the cycles increased under the test conditions of the applied stress level of $\sigma_{max}/\sigma_b =$ 0.3–0.6 at the frequency of 5 Hz and the applied stress level of $\sigma_{max}/\sigma_b = 0.3$ at the frequency of 100 Hz. However, under the test condition of applied stress level of $\sigma_{max}/\sigma_b = 0.2$, the propagation of the cracks that were initiated at the specimen edges was not observed up to 10^8 cycles at the frequency of 100 Hz and up to 2×10^7

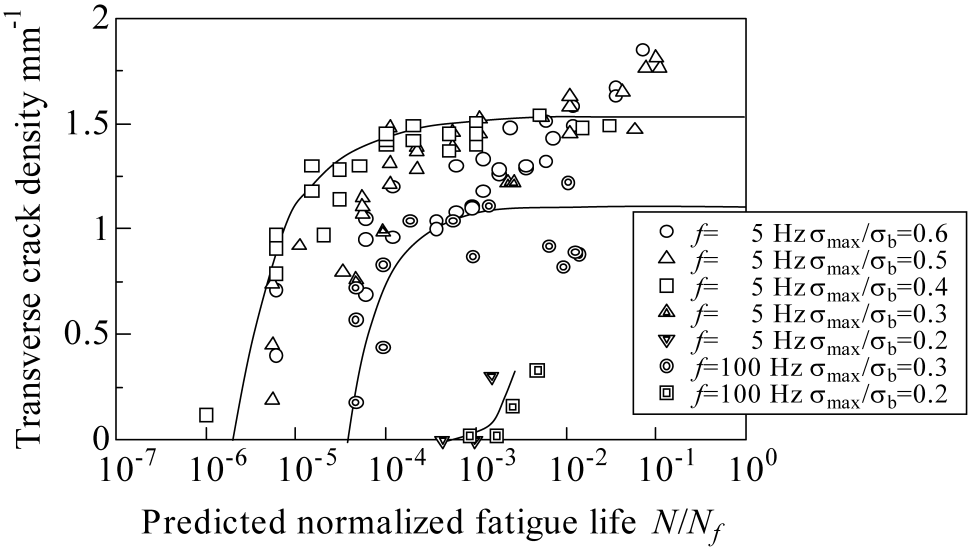

Figure 7. Transverse crack density observed at specimen edge as a function of normalized fatigue life.

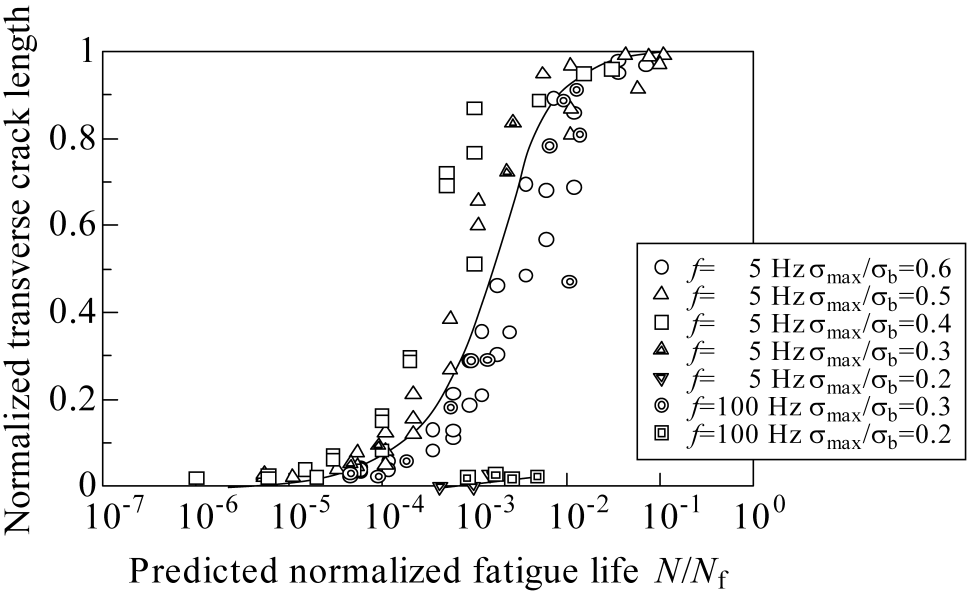

Figure 8. Normalized transverse crack length propagating in width direction of specimen as a function of normalized fatigue life.

cycles at the frequency of 5 Hz. From the results of both Figs 7 and 8, no difference in transverse crack growth due to the frequency was observed.

In this study, a transverse crack propagating to the width direction of the specimen was evaluated quantitatively. However, the interaction between the matrix cracks

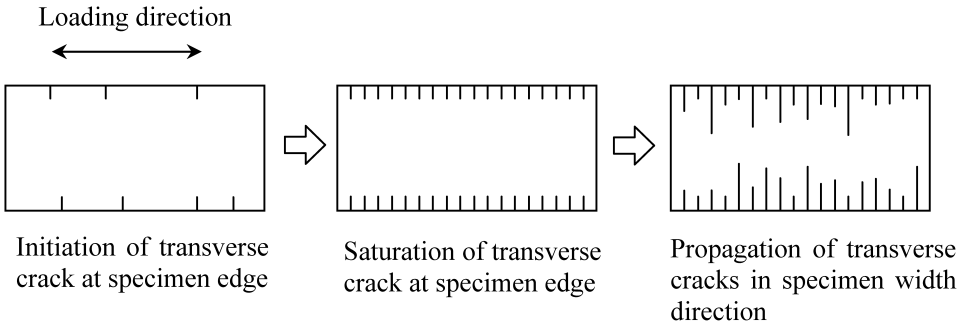

Figure 9. Behavior of transverse crack propagation in CFRP laminates of stacking sequence $[-45/0/45/90]_S$ subjected to cyclic loading.

on the 45 deg ply or −45 deg ply and the delamination was not considered in the analysis.

4.2. Evaluation of transverse crack propagation

Yokozeki *et al.* [16] researched transverse cracks propagating in the width direction of specimen with several CFRP, cross-ply laminates and quasi-isotropic laminates. They applied the study according to Nairn [18], who calculated the energy release rate associated with transverse crack growth taking into account the effect of the residual thermal stress of multi-ply laminates. In the present study, we calculated the energy release rate associated with transverse crack propagation in the width direction of the specimen referring the study conducted by Yokozeki *et al*. [16].

From the study conducted by Nairn [18], the energy release rate associated with transverse crack growth is expressed as

$$G = \frac{V}{2}\left(\sigma_0 - \Delta\alpha_{xx} E_{xx}^{(u)}(1-\nu_1)T_r\right)^2 \frac{\mathrm{d}}{\mathrm{d}A}\left(\frac{1}{E_{xx}^*}\right), \tag{6}$$

where V is the volume of the specimen, ν_1 is the volume fraction of the plies where the transverse cracks exist, σ_0 is the applied stress and A is the fracture area. Also, $\Delta\alpha_{xx} = \alpha_{xx}^{(1)} - \alpha_{xx}^{(u)}$ is the difference between the axial direction thermal expansion coefficients of the 90 deg ply and undamaged plies, and $T_r = T_s - T_0$ is the difference between the test temperature T_s and the residual stress-free temperature T_0. Moreover, $E_{xx}^{(u)}$ and E_{xx}^* are the rule-of-mixtures axial modulus of the uncracked plies and the effective laminate modulus in the axial direction, respectively. As Yokozeki *et al*. [16] defined, it was assumed that each transverse crack propagated in the width direction with the same length by averaging each transverse crack length and there was no the new edge cracking. The analytical model is shown in Fig. 10. In this study, V and $\mathrm{d}A$ are expressed as

$$V = 2(t_1 + t_2) \cdot L \cdot (2W), \quad \mathrm{d}A = 2(\mathrm{d}\bar{a}_t \cdot 2t_1 \cdot n), \tag{7}$$

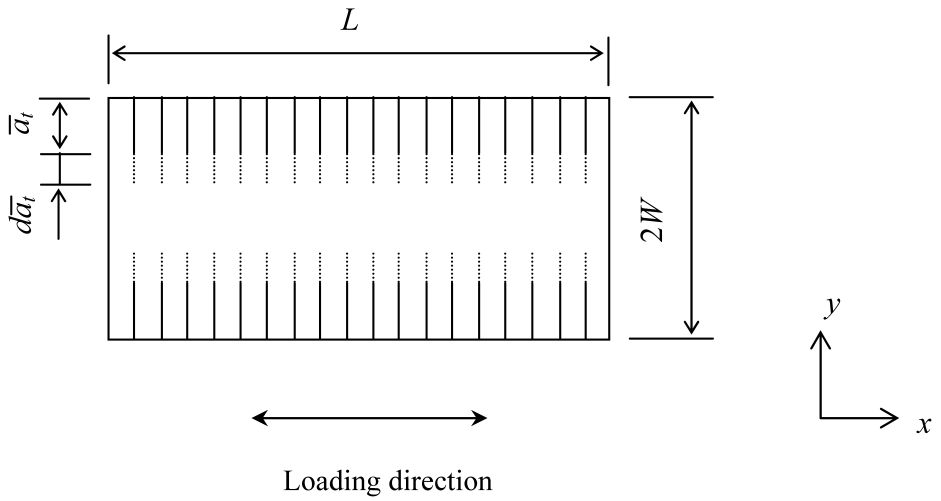

Figure 10. Analytical model for calculation of energy release rate associated with transverse cracks propagating in specimen width direction.

where t_1 and t_2 are the specimen thickness of 90 deg ply and undamaged plies, respectively; L and W are the gage length and width of the specimen. Then, $\bar{a}_t$ and n express the averaged transverse crack length and the number of transverse cracks within gage length, L. Moreover, with the rule of mixtures, the modulus of the laminates where the transverse cracks exist is expressed as

$$E^*_{xx} = (E_c - E_0)\frac{\bar{a}_t}{W} + E_0, \tag{8}$$

where E_c and E_0 mean the axial laminate modulus that transverse cracks pass through the specimen width and the undamaged laminate modulus in the axial direction. Then, the differentiation of inverse in the equation (8) is

$$\mathrm{d}\left(\frac{1}{E^*_{xx}}\right) = -\frac{1}{W}(E_c - E_0)\cdot \mathrm{d}\bar{a}_t \cdot \left[(E_c - E_0)\frac{\bar{a}_t}{W} + E_0\right]^{-2}. \tag{9}$$

By substituting equations (7) and (9) into equation (6), the energy release rate associated with transverse crack propagation to the width direction of the specimen is expressed as

$$G_t = \frac{t_1 + t_2}{2\rho_1 t_1}\left(\sigma_0 - \frac{t_2 E^{(u)}_{xx}}{t_1 + t_2}\Delta\alpha_{xx}T_r\right)^2 \cdot \left(\frac{E_0 - E_c}{(E^*_{xx})^2}\right), \tag{10}$$

where ρ_1 is the crack density of 90 deg ply. It is found that the calculated energy release rate is expressed only by the change of stiffness and does not depend upon the transverse crack length.

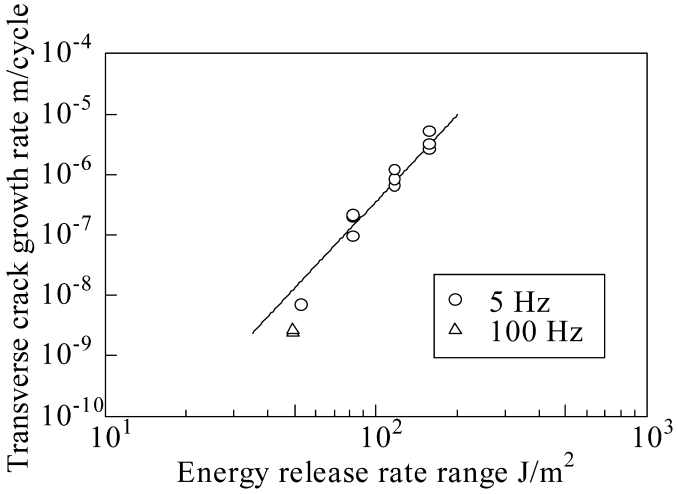

Figure 11. Transverse crack growth rate as a function of energy release rate range.

Following Tong *et al.* [19], the relation between the transverse crack growth rate and the energy release rate range is expressed with the modified Paris law as

$$\frac{\mathrm{d}\bar{a}_t}{\mathrm{d}N} = A(\Delta G_t)^{\gamma}, \tag{11}$$

$$\Delta G_t = G_t|_{\sigma=\sigma_{\max}} - G_t|_{\sigma=\sigma_{\min}}, \tag{12}$$

where N, A and γ are the number of cycles and constants, respectively. The transverse crack growth rate as a function of the energy release rate range is shown in Fig. 11. From the results, it was found that the transverse crack propagation could be evaluated by the modified Paris law within this study. In Fig. 11, the results under the test condition of the applied stress level of $\sigma_{\max}/\sigma_{\mathrm{b}} = 0.2$ were not included because the crack propagation under the test condition was not observed. That is to say, Fig. 11 evaluates the results of the applied stress level of $\sigma_{\max}/\sigma_{\mathrm{b}} =$ 0.3–0.6. As shown in Fig. 11, it was observed that the transverse crack growth rate delayed under the applied stress level of $\sigma_{\max}/\sigma_{\mathrm{b}} = 0.3$. Moreover, as shown in Fig. 8, the transverse crack propagation was not observed up to 10^8 cycles under the applied stress level of $\sigma_{\max}/\sigma_{\mathrm{b}} = 0.2$. Considering these results, it is thought that a threshold exists for the propagation of transverse crack. In this study, delamination growth was also observed together with transverse crack propagation; however, this analysis does not consider the interaction between the transverse crack and the delamination growth.

4.3. Behavior of delamination growth

Delamination growth was observed as shown in Fig. 12 with soft X-ray photography and a 3D ultrasonic inspection system. Then, Fig. 13 shows the delamination area

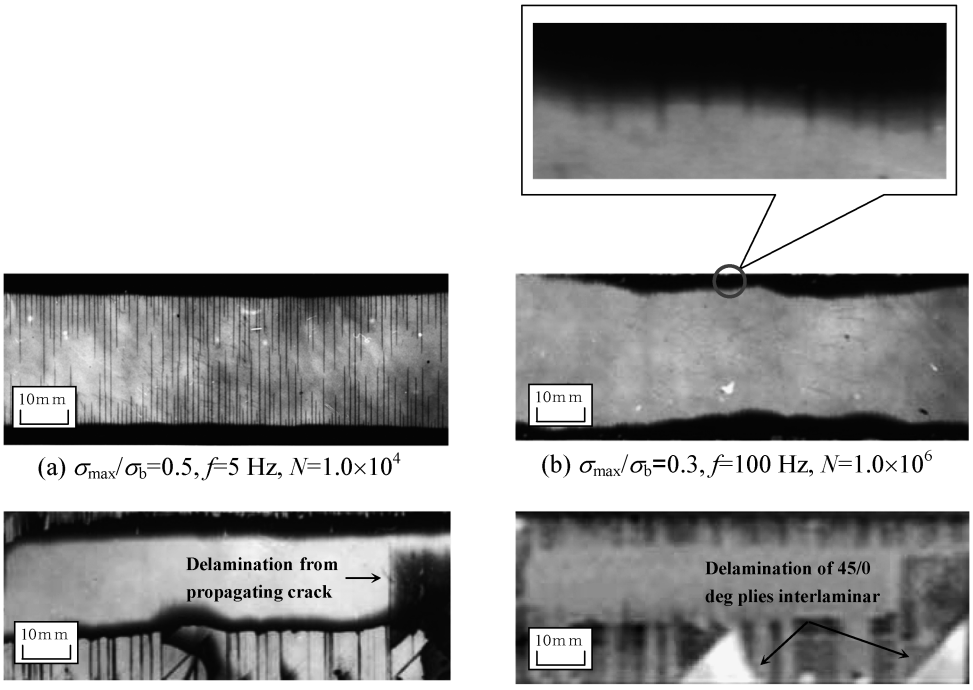

(a) σ_{max}/σ_b=0.5, f=5 Hz, N=1.0×10^4 (b) σ_{max}/σ_b=0.3, f=100 Hz, N=1.0×10^6

(c) σ_{max}/σ_b=0.3, f=100 Hz, N=9.0×10^6 (d) σ_{max}/σ_b=0.3, f=100 Hz, N=9.0×10^6

Figure 12. Damage behavior observed with soft X-ray photography [(a), (b), (c)] and 3D ultrasonic inspection system [(d)].

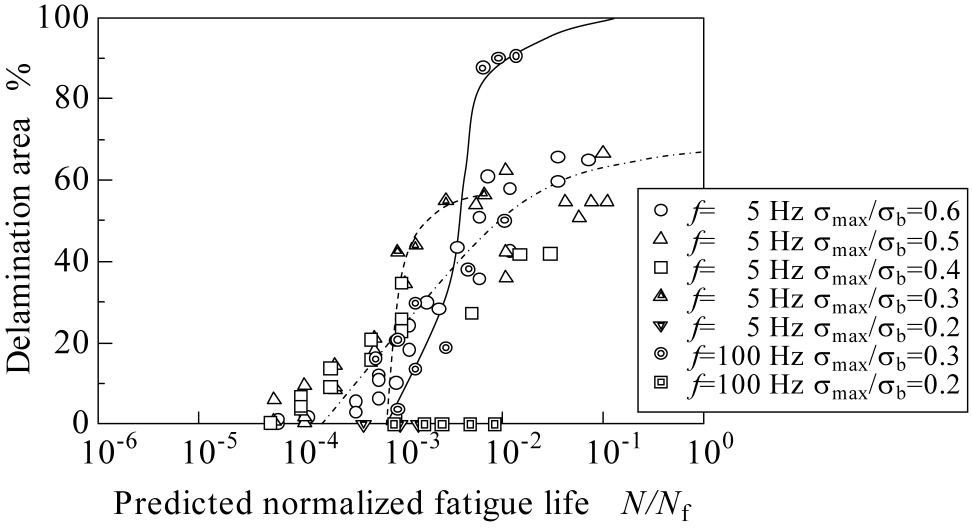

Figure 13. Delamination area as a function of normalized fatigue life.

as a function of normalized fatigue life. From these results, it was observed that the delamination growth behavior varied with the applied stress level.

First, when the fatigue test was conducted under the applied stress levels of $\sigma_{\max}/\sigma_{\mathrm{b}} = 0.4$–$0.6$, the delamination propagated in the width direction after the transverse cracks had propagated in the width direction of the specimen as shown in Fig. 12(a), while it was observed that the transverse cracks and delamination propagated at the same time when the fatigue test was conducted under the conditions of the applied stress level of $\sigma_{\max}/\sigma_{\mathrm{b}} = 0.3$ and at a frequency of 100 Hz as shown in Fig. 12(b) and 12(c). The detailed view shown in Fig. 12(b) revealed that the delamination propagated along the transverse crack tip and did not propagate over the transverse cracks.

Second, under the conditions of the applied stress level of $\sigma_{\max}/\sigma_{\mathrm{b}} = 0.3$ and at a frequency of 100 Hz, the delamination that initiated from the propagating transverse crack and the remarkable delamination that was caused at the interlaminar area of 45/0 deg plies were observed as shown in Fig. 12(c) and 12(d), respectively. The following points were thought to provide the reason. When the fatigue test was conducted at a frequency of 100 Hz, the temperature of the specimen rose, and then the residual thermal stress was relaxed. Thus, the transverse crack growth rate delayed, as clearly seen from the results shown in Fig. 11. The transverse crack growth rate under the test condition at a frequency of 100 Hz is smaller than that under the test condition at the frequency of 5 Hz despite the same applied stress level. Moreover, as shown in Fig. 12(b), delamination did not propagate over the transverse cracks. Therefore, it was thought that the delamination growth to the width direction of the specimen was depressed due to the delay of transverse crack growth rate, and then the delamination growth from the propagating crack and the 45/0 plies interlaminar was promoted.

4.4. Evaluation of delamination growth

In this study, delamination growth was evaluated quantitatively with the approach proposed by O'Brien [20]. The energy release rate associated with delamination growth is expressed as

$$G_d = \frac{t\varepsilon_0^2}{2}(E_{\mathrm{LAM}} - E^*), \tag{13}$$

$$\frac{\mathrm{d}\bar{a}_d}{\mathrm{d}N} = C_d(\Delta G_d)^{\gamma_d}, \tag{14}$$

where t and ε_0 are the thickness and the applied strain of the specimen, respectively, and E_{LAM} and E^* are the axial laminate stiffness calculated from laminated plate theory and the axial stiffness of a laminate completely delaminated along one or more interfaces. Also, C_d, and γ_d are constants; moreover, $\bar{a}_d$ and N are the averaged delamination length and the number of cycles, respectively. Figure 14 shows the results calculated from equations (13) and (14).

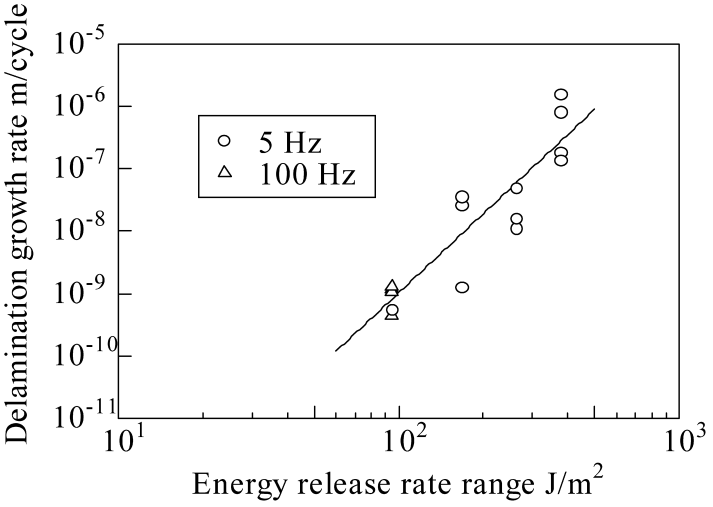

Figure 14. Delamination growth rate as a function of energy release rate range.

From the results, it was found that the delamination growth could be evaluated by the modified Paris law within this study. However, the delamination was not observed up to 10^8 cycles under the applied stress level of $\sigma_{max}/\sigma_b = 0.2$ as shown in Fig. 13, so the results were not considered.

5. CONCLUSION

In this study, the high-cycle fatigue characteristics of quasi-isotropic CFRP laminates were investigated with the following results. First, it was observed that the transverse crack growth rate delayed under the test condition at the applied stress level of $\sigma_{max}/\sigma_b = 0.3$. Then, considering the results that a transverse crack did not propagate to the width direction in the specimen up to 10^8 cycles under the test condition at the applied stress level of $\sigma_{max}/\sigma_b = 0.2$, it was thought that a threshold exists for propagation of the transverse cracks. Moreover, it was observed that delamination growth to the width direction in the specimen was inhibited by the delay of the transverse crack propagation under the test conditions at a frequency of 100 Hz and an applied stress level of $\sigma_{max}/\sigma_b = 0.3$. This served to promote delamination growth from the transverse crack propagating in the width direction or from the interlamination of the 0/45 deg plies.

Acknowledgements

The authors wish to thank Dr. Ogasawara and Dr. Yokozeki of Japan Aerospace Exploration Agency for help to use the soft X-ray photography, and to acknowledge Professor S. Mark Spearing for useful discussion on this subject. This work was supported in a part of the 21st century Center of Excellence program.

REFERENCES

1. T. K. O'Brien, M. Rigamonti and C. Zanotti, Tension fatigue analysis and life prediction for composite laminates, *Int. J. Fatigue* **11**, 379–393 (1989).
2. J. Tong, Fatigue crack growth in composite laminates, in: *Recent Advances in Fracture*, R. K. Mahidhara, A. B. Geltmacher, P. Matic and K. Sadananda (Eds), pp. 251–260. TMS, Warrendale, PA, USA (1997).
3. J. Tong, Characteristics of fatigue crack growth in GFRP laminates, *Internat. J. Fatigue* **24**, 291–297 (2002).
4. S. Kobayashi and N. Takeda, Experimental and analytical characterization of transverse cracking behavior in carbon/bismaleimide cross-ply laminates under mechanical fatigue loading, *Composites Part B – Eng* **33**, 471–478 (2002).
5. L. Boniface and S. L. Ogin, Application of the Paris equation to the fatigue growth of transverse ply cracks, *J. Compos. Mater.* **23**, 735–754 (1989).
6. K. L. Reifsnider and A. Talug, Analysis of fatigue damage in composite laminates, *Internat. J. Fatigue* **2**, 3–11 (1980).
7. M. Spearing, P. W. R. Beaumont and M. F. Ashby, Fatigue damage mechanics of notched graphite-epoxy laminates, *ASTM STP* **1110**, 617–637 (1991).
8. Z. Hashin, Analysis of cracked laminates: a variational approach, *Mech. Mater.* **4**, 121–136 (1985).
9. J. A. Nairn, The strain energy release rate of composite microcracking: a variational approach, *J. Compos. Mater.* **23**, 1106–1119 (1989).
10. J. A. Nairn, Matrix microcracking composites, in: *Polymer Matrix Composites*, R. Talreja and J.-A. E. Månson (Eds), pp. 403–432. Elsevier, Amsterdam (2000).
11. L. N. McCartney, Stress transfer mechanics for ply cracks in general symmetric laminates, *NPL Report CMMT (A)* **50**, 1–47 (1996).
12. P. Gudmundson and W. Zang, An analytic model for thermoelastic properties of composite laminates containing transverse matrix cracks, *Internat. J. Solids Struct.* **30**, 3211–3231 (1993).
13. J. E. Masters and K. L. Reifsnider, An investigation of cumulative damage development in quasi-isotropic graphite/epoxy laminates, *ASTM STP* **775**, 40–62 (1982).
14. S. Liu and J. A. Nairn, Fracture mechanics analysis of composite microcracking: Experiment results in fatigue, in: *Proc. Fifth Tech. Conf. Compos. Mater.*, Michigan, pp. 287–295. American Society for Composites (1990).
15. N. Takeda, S. Kobayashi, S. Ogihara and A. Kobayashi, Effects of toughened interlaminar layers of fatigue damage progress in quasi-isotropic CFRP laminates, *Internat. J. Fatigue* **21**, 235–242 (1999).
16. T. Yokozeki, T. Aoki and T. Ishikawa, Fatigue growth of matrix cracks in the transverse direction of CFRP laminates, *Compos. Sci. Technol.* **62**, 1223–1229 (2002).
17. A. Hosoi, H. Kawada and H. Yoshino, Fatigue characteristics of quasi-isotropic CFRP laminates subjected to variable amplitude cyclic two-stage loading, *Internat. J. Fatigue* **28**, 1284–1289 (2006).
18. J. A. Nairn, Fracture mechanics of composite with residual thermal stresses, *J. Appl. Mech.* **64**, 804–810 (1997).
19. J. Tong, F. J. Guild, S. L. Ogin and P. A. Smith, On matrix crack growth in quasi-isotropic laminates-I. Experimental investigation, *Compos. Sci. Technol.* **57**, 1527–1535 (1997).
20. T. K. O'Brien, Characterization of delamination onset and growth in a composite laminate, *ASTM STP* **775**, 140–167 (1982).